Role of autophagy-related proteins and cellular microRNAs in chikungunya and dengue virus infection

Echavarria Consuegra, Sandra

DOI:
10.33612/diss.108290836

CHAPTER 3

siRNA-based evaluation of the role of autophagy-related proteins and autophagy receptors in dengue virus infection

Liliana Echavarria-Consuegra[1], Mario Mauthe[2], Fulvio Reggiori[2], Jolanda M. Smit[1]

[1]Department of Medical Microbiology and Infection Prevention, University Medical Center Groningen, University of Groningen, Groningen, The Netherlands
[2]Department of Cell Biology, University Medical Center Groningen, University of Groningen, The Netherlands

Abstract

Dengue virus (DENV) is a mosquito-borne flavivirus that is responsible for approximately 390 million human infections yearly. Of these, roughly 96 million individuals develop an acute febrile illness of which 0.5 to 1 million people develop a more severe disease which is fatal in approximately 20,000 cases. The constant interplay between the virus and the host determines the outcome of infection. In infected cells, the degradative pathway of autophagy is often triggered as an antiviral stress response, yet many viruses have evolved to utilize components of the autophagy pathway for their benefit. Indeed, the presence of the non-structural DENV proteins in infected cells was shown to induce autophagy. On the other hand, however, other studies suggested that degradation of lipid droplets by autophagy and certain autophagy-related proteins (ATG) promote DENV infection. Here, we aimed at determining the role of the entire set of core ATG proteins and several autophagy receptors in DENV infection using an image-based siRNA screen. First, we describe the optimization and validation of the screening approach. Thereafter, the screen was performed and the results revealed that most factors had only minor effects on DENV infection in Huh7 cells. In total, 11 single ATG knockdowns were found to significantly enhance DENV infection, which suggests that these proteins restrict DENV replication. From the identified hits, NBR1 and ATG4C had the most pronounced effect. Future studies should be performed to validate their role in DENV infection and their mechanism of action.

1. Introduction

Dengue virus (DENV) is the causative agent of dengue fever, which continues to be the most important arthropod-borne viral human disease in terms of incidence and public health impact (1,2). DENV belongs to the genus *Flavivirus* and is transmitted to humans through the bites of female *Aedes* spp. mosquitoes, which are now widely dispersed in all continents, including North America and Southern Europe (3). DENV infection can lead to a wide range of clinical manifestations, ranging from a self-limiting mild febrile illness to life-threatening conditions such as shock, liver failure or severe haemorrhages (4,5). A DENV-attenuated chimeric vaccine has recently been licensed (6), however, its performance has been highly debated due to exacerbation of the disease symptoms in vaccinated individuals undergoing a natural infection, potentially as a consequence of antibody-dependent enhancement (7). Furthermore, there are no antiviral drugs available that specifically lower the disease burden. For the rational design of novel therapeutic and prophylactic interventions a thorough understanding of the virus-host interactions is warranted.

DENV particles are enveloped and contain a nucleocapsid which is composed of the capsid protein (C) and the viral genomic RNA (8,9). The envelope contains two structural proteins, the membrane (M) and the envelope (E) protein (8,9). The viral genome is a capped, single-stranded positive-sense RNA molecule of 11 kb in length, which encodes for 3 structural proteins (C, E, prM) and 7 non-structural (NS) proteins (NS1, NS2A/B, NS3, NS4A/B, NS5) (10,11). The replicative cycle of DENV initiates when the E protein attaches to cell receptors, thereby triggering internalization of the virion via clathrin-mediated endocytosis (12,13). Following uptake and endosome maturation, E-mediated membrane fusion occurs, and the nucleocapsid is delivered into the cytoplasm (14). Upon dissociation, the RNA genome is translated into a single polyprotein in close proximity to the ER (15). The NS proteins facilitate RNA replication (16–19). Virions are assembled by inward budding of newly formed nucleocapsids into the ER membrane that express the E and precursor M viral proteins (15). Progeny virions mature by transport through the secretory pathway prior to extracellular release by exocytosis (20).

Once a cell is infected, multiple pathways are triggered or inhibited, which will eventually determine the fate of the cell and the virus. Autophagy is a cellular degradative pathway, often activated in infected cells as part of the stress response (21). Even though the term autophagy encompasses several pathways, macroautophagy is the one that has been mostly studied (22). Macroautophagy (hereafter referred to as autophagy) involves the formation of double membrane vesicles, known as autophagosomes, which surround intracellular structures and compartments for turnover after fusion with lysosomes (22). Biogenesis of autophagosomes is orchestrated by the so-called ATG proteins (23). Autophagy is initiated once the ULK kinase complex is activated by upstream signals triggered for example by nutrient and/or energy depletion, or by viral infections (24,25). Together with the class III phosphatidylinositol 3-kinase complex and the components of the ATG9A system, the active ULK complex mediates the formation of the phagophore, a membranous cistern that will eventually become an autophagosome. Two ubiquitination-like systems participate in the subsequent steps of the autophagosome

biogenesis. The first ubiquitination-like system, formed by ATG7 and ATG10, generates an ATG12-ATG5 conjugate, which associates with ATG16L1 (26). The second system leads to the conjugation of LC3-I to phosphatidylethanolamine (PE), which is mediated by ATG7, ATG3 and the ATG12-ATG5/ATG16L1 complex (26). PE-conjugated LC3-I, i.e., LC3-II, supports phagophore elongation and closure (27). Furthermore, autophagy receptors such as p62 and NBR1, are able to interact with LC3-II in order to direct cargoes into autophagosomes for degradation, in a process known as selective autophagy (28). After closure, autophagosomes fuse with endosomes/lysosomes, and lysosomal enzymes degrade the cargo contained within these organelles (29,30).

It has been shown that the NS proteins of DENV trigger autophagy during infection (31). Furthermore, active lysosomal degradation of p62 has also been observed in DENV-infected cells, suggesting that autophagy may act as an antiviral pathway (32). ATG proteins like ATG12, BECLIN1 and LC3B, however, have been shown to promote DENV replication in several *in vitro* models (31,33–35). These data appears contradictory, yet, recent data have revealed that ATG proteins can also have non-canonical functions unrelated to autophagy (36–38). As a result, the overall importance of autophagy and the ATG proteome during DENV infection still has to be fully understood.

The goal of this study was to carry out a comprehensive examination of the entire ATG proteome to determine whether core ATG genes and selected autophagy receptors play a role in DENV infection. To this aim, we designed and run an image-based siRNA screen targeting the mRNAs of 50 ATG and autophagy receptor genes. We chose Huh7 cells as a model as hepatocytes are targets of DENV during infection. We found 11 significant hits that enhanced DENV infection and two of them, NBR1 and ATG4C, were further investigated. Overall, our screen data suggests that an intact autophagy pathway is not required for DENV infection in Huh7 cells and implies that the few ATG proteins identified control infection through unconventional mechanisms.

2. Materials and methods

Cell lines. Huh7 cells (JCRB0403) were kindly provided by Tonya Colpitts (University of South California School of Medicine, USA) and were maintained in DMEM, high glucose, GlutaMAX™ Supplement (Gibco). Baby hamster kidney (BHK) clone 21 cells (ATCC CCL-110) were cultured in RPMI 1640 medium (Gibco). BHK-21 clone 15 were kindly provided by Richard Kuhn (Purdue University, USA) and were cultured in DMEM (Gibco), supplemented with 100 µM of non-essential amino acids (Gibco) and 10 mM Hepes (Gibco). *Aedes albopictus* C6/36 cells (ATCC CRL-1660) were maintained in minimal essential medium (Invitrogen), supplemented with 25 mM Hepes (Gibco), 0.075% sodium bicarbonate (Gibco), 200 mM glutamine (Gibco) and 100 µM non-essential amino acids (Gibco). All media was supplemented with 10% heat inactivated fetal bovine serum (FBS, Lonza) and 100 U/ml penicillin/streptomycin (Gibco). Mammalian cell lines were maintained at 37°C in humidified atmosphere containing 5% CO_2. Mosquito C6/36 cells were cultured at 28 ºC and 5% CO_2.

Virus production and characterization. Recombinant GFP-DENV, in which the GFP sequence was inserted upstream of the capsid-encoding sequence, was generated from

the cDNA clone pFK-DV-G2A 16681, generously provided by Ralf Bartenschlager (University of Heidelberg, Germany) (39). Briefly, purified plasmid was linearized using *Xba*I (NEB) and used for RNA synthesis using SP6 polymerase (NEB). Capped transcripts were electroporated into BHK-21 cells (Biorad gene pulser Xcell machine; 850V, 25µF, no resistance). At 48 h post-electroporation, the cell supernatant was harvested, clarified by low speed centrifugation and used to infect C6/36 cells at a multiplicity of infection (MOI) of 0.1. Working stocks of virus were collected at 72 hours post-infection (hpi), clarified and used for all infection experiments. The virus preparation was characterized by standard plaque assay in BHK-15 cells to determine the number of plaque forming units (PFU/ml) and by RT-qPCR to determine the number of genome equivalent copies (GEC/ml), as previously described (40).

Validation and optimization of the screen conditions. This screening setup was previously used by our laboratory to screen other viruses in different cell lines (36). To adapt the previously established knock-down methods, Huh7 cells were reverse transfected in 96-well plates using 2 pmol of siRNA and 0.1µl of Lipofectamine RNAiMax transfection reagent (Invitrogen) per well, in a final volume of 100 µl following manufacturer's instructions, for 48 h. Cells were then lysed using the cells to CT kit (Invitrogen) followed by reverse transcription reaction and qPCR using specific primers for ARF1, GBF1, and GAPDH following manufacturer's instructions. GAPDH was used as the reference housekeeping gene. Quantification was performed by means of the delta-delta CT method.

To optimize the screen conditions, 3000 Huh7 cells were seeded per well in a 96-wells plate in a final volume of 100 µl and infected with DENV at MOI 5 and 10, 48 h after seeding. For infection, 50 µl of medium was replaced by 50 µl of virus suspension in complete medium containing 10% FBS. At 24, 28, 32 and 48 hpi, cells were fixed with 4% paraformaldehyde (PFA) and nuclei were stained with Hoechst33342 (Sigma-Aldrich). Automated microscopy was performed at the Cell Screening Core of the University Medical Centre Utrecht, The Netherlands. Plates were imaged in a Cellomics ArrayScan VTI HCS Reader (Thermo Fisher Scientific) using Hoechst and FITC filters, and 10x lens for automated image acquisition. The Hoechst channel was used to set the autofocus and to determine the cell number, while the GFP signal due to the infection was detected using the FITC filter. An equal fixed exposure time was automatically set for all the samples (36). GFP expression was analysed in approximately 1500 cells using the Cellomics SpotDetector V3 algorithm. Three parameters were measured and calculated: 1) GFP intensity per cell, 2) percentage of GFP-positive cells and 3) average GFP intensity in GFP-positive cells.

siRNA-based screen. For the primary siRNA screen, a customized ON-TARGETplus SMARTpool human siRNA library (Dharmacon, Horizon™) targeting the mRNA of 50 ATG and autophagy receptor genes (Table S1), either singularly or in combination, was generated. The siRNAs were pre-spotted in 96-well plates using a total amount of 2 pmol for single gene knock-down, 3 pmol for 2 genes, 4.5 pmol for 3 genes, and 6 pmol for 4 genes. Reverse transfection was performed using 0.1µl of Lipofectamine RNAiMax transfection reagent (Invitrogen) per well following manufacturer's instructions. After 20 min, Huh7 cells were seeded in complete culture medium to a final volume of 100 µl

(36). At 48 h post-transfection, cells were infected at MOI 10. At 28 hpi, the cells were fixed, stained and images were acquired, as described for the optimization experiments.

Analysis of the screen data. Measurements from four independent experiments were standardized using the robust Z-score calculation. The median Z-score and the standard deviation of the mean were then determined. Z-score values below −1.96 and above 1.96 were considered statistically significant. Fold changes as compared to the siScramble of each independent experiment were also calculated, and the averages of the replicas are represented in a heat map. Fold changes calculated for each one of the parameters of the screen were used to create a heat map in Microsoft Excel 2016 using conditional formatting.

Validation: siRNA-mediated silencing and infection. Individual siRNAs targeting NBR1 (ID: LU-010522-00-0002), ATG4C (ID: LU-005788-00-0002), or non-targeting siRNA (siScramble, ID: D-001810-10) were purchased from Dharmacon (Horizon™). Reverse transfection of Huh7 cells in 24 well plates was performed using 0.5 µl of Lipofectamine RNAiMAX (Invitrogen), in a total volume of 500 µl and at a final siRNA concentration of 20 nM. At 48 h post-transfection, cells were infected with DENV at an MOI of 10 for 28 h. At this time point, cells were detached with 0.5% trypsin-EDTA (Gibco) and washed once with FACS buffer (PBS, 5% FBS, 1% EDTA). Subsequently, the cells were fixed with 4% PFA and suspended in FACS buffer. To detect the number of infected cells, GFP expression was assessed by flow cytometry. In all experiments, 10,000 events per condition were acquired in a BD FACSVerse instrument (BD Biosciences) and analysed using Kaluza analysis 2.1 software (Beckman Coulter).

Statistical analysis. GraphPad Prism software version 5 was used to statistically analyse and depict all the data. Values are presented as mean ± SEM. Statistical differences were determined using two-tailed student's *t*-test or dependent *t*-test. Pearson correlations were calculated to measure the linear statistical association between quantitative variables or data from independent experiments. The coefficient correlation (Pearson R) measures the degree of association. A p value ≥0.05 was considered as statistically significant.

3. Results

To systematically and comprehensively study the functional connection between DENV infection and the core ATG proteins or selected autophagy receptors, an image-based siRNA screen targeting a large variety of genes was designed. Hepatoma-derived Huh7 cells were chosen as a model, as hepatocytes are natural targets during infection (41), and most of the previous studies on the regulation of autophagy in DENV infection used this cell line (32,34,35). We used siRNA pools for downregulation to reduce the probability of off-target effects often encountered for individual siRNA probes (42). The library consisted of 50 siRNA pools targeting 50 different individual core ATG genes and few autophagy receptors (Table S1). We also decided to make combinations of siRNA pools to silence different isoforms of the same protein to target redundant functions. The siRNA pools were reverse-transfected in Huh7 cells as described in Materials and

Methods. We have successfully used this screening approach before to evaluate the role of ATG proteins in the replication of 6 other RNA and DNA viruses in human cells (36). In the context of the previous study, we also showed that the applied strategy was effective, as clear changes in p62 and LC3 puncta formation were induced, which is indicative for inhibition of autophagy (36). In this screen cells were challenged with a GFP-reporter DENV strain and the GFP signal was used to determine 1) the number of infected cells (GFP-positive cells), and 2) the level of viral replication in infected cells (GFP intensity in infected cells) (39). As a third read-out, the total GFP intensity per well was measured. Prior to performing the screen for DENV, however, several parameters were optimized. First, the knockdown efficiency of two randomly selected proteins, i.e., ARF1 and GBF1, was corroborated in Huh 7 cells by analysing their mRNA levels by RT-qPCR upon transfection with specific siRNA pools (Fig. 1A). In both cases, transfection of 20 nM siRNAs using 0.1µl of the transfection reagent for 48 h led to a clear reduction of the respective RNA transcripts (up to 90%) as compared to the cells transfected with the control siRNA (siScramble), confirming the effectivity of the knockdown approach. Second, we decided to select for a condition that would allow us to monitor both enhancement and inhibition of infection under conditions of siRNA-mediated silencing. Furthermore, we searched for the condition with the best GFP signal to noise ratio within one round of replication to ensure a high sensitivity of the assay. To select the condition that fulfils the above criteria, Huh7 cells were infected at MOI 5 and 10 with GFP-reporter DENV and GFP expression was assessed by automated high-throughput microscopy at various time-points after infection (24-48h). The infection rate was determined via a standard algorithm which identified cells by Hoechst staining and scored infected cells on the basis of overlap in Hoechst and GFP signal (e.g., Fig. 1B, analysis overlay). Furthermore, the mean fluorescence intensity of GFP per well was determined and compared to mock-infected wells to calculate the signal to noise ratio. At 24 hpi, 13.2%, and 21.5% of the cell population was infected following infection at MOI 5 and 10, respectively. At 28 hpi, the percentage of infected cells was very similar, i.e., 11.9% and 22.3% for MOI 5 and 10, respectively. Furthermore, the signal to noise ratio of the infected cells as compared to the mock-infected cells, increased in an MOI- and time-dependent manner (Fig. 1C). At 24 hpi, the ratio was 1.9 and 3.4 following infection at MOI 5 and 10, respectively. At 28 hpi, the ratio increased to 2.3 and 4.3 at MOI 5 and 10, respectively. At latter time-points, even higher ratios were observed. In all conditions tested, the GFP signal was higher than background (mock-infected cells). Previous analysis of the growth kinetics of DENV on Huh7 cells in our laboratory revealed that initial detectable DENV production is at 18 hpi with bulk production at 24-30 hpi, indicating that one round of replication roughly takes 18-24 hrs (43). Furthermore, GFP expression is detectable from 12 hpi. Thus, assaying GFP expression at 28 hpi still reflects one round of replication. Collectively, on the basis of the above tests, we selected MOI 10 and 28 hpi as the best conditions to assess GFP-report DENV in our siRNA-based screen.

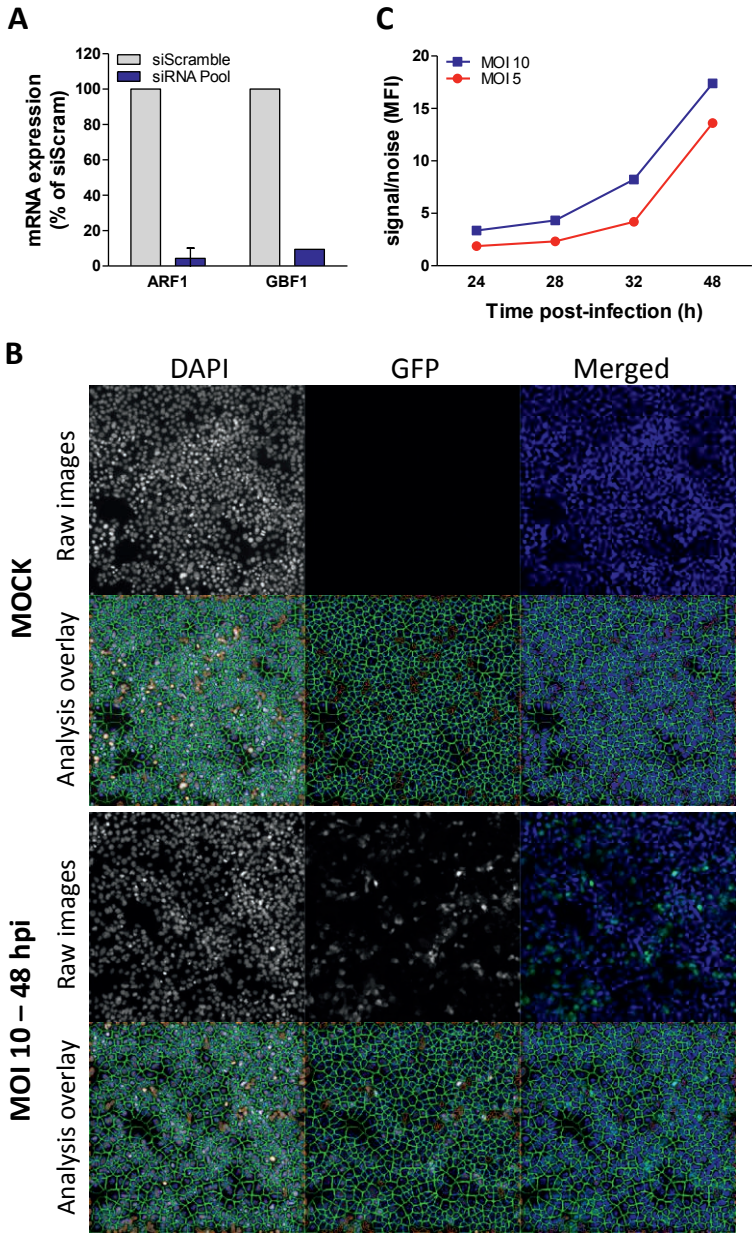

Figure 1. Optimization of an image-based siRNA screen to determine the role of the core ATG proteins and selected autophagy receptors in DENV infection. (A) Bar plot showing the extent of siRNA-induced mRNA silencing of ADP-ribosylation factor 1 (ARF1) and Golgi-specific brefeldin A-resistance guanine nucleotide exchange factor 1 (GBF1) in Huh7 cells as quantified by RT-qPCR. Data is shown relative to that of siScramble-transfected control cells, based on n=1. **(B - C)** Huh7 cells were seeded in 96-well plates and infected with GFP-DENV at the indicated MOIs and harvested at the indicated time-points. **(B)** Representative images of mock-infected cells and cells infected with GFP-DENV at MOI 10 for 48 h. Data analysis is shown for each condition. **(C)** Line graph showing the signal to noise ratio based on the GFP mean fluorescence intensity in infected wells as compared to mock-infected cells. Data is based on n=1 and at least 4 technical replicates.

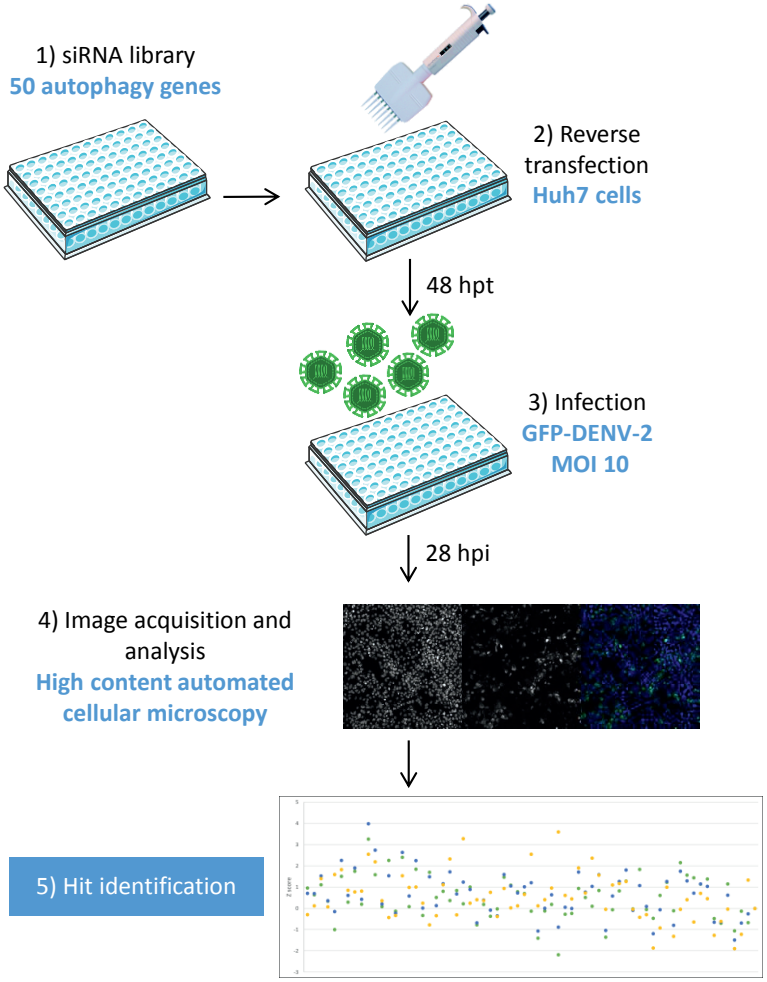

Figure 2. Schematic representation of the siRNA screen experimental design. 1) siRNA pools were pre-spotted in 96 well plates. 2) After reconstitution, transfection reagent and Huh7 cells were added to the wells. Plates were incubated for 48 h to allow siRNA-mediated silencing. 3) Reverse-transfected cells were infected with GFP-DENV-2 at MOI 10. 4) At 28 hpi, the plates were fixed and nuclei stained prior image acquisition and analysis. 5) Hit identification and data analysis.

The screen was performed in quadruplicate as depicted in Fig. 2. First, we evaluated the total cell number per well to analyse potential cytotoxic effects of the siRNA treatment (Fig. 3A). Because we observed that none of the siRNA transfections drastically changed the average cell number (i.e., >±30% change when compared to cells transfected with the siScramble), none of the siRNA pools were excluded from further analysis (Fig. 3A). The total cell number per well, expressed as percentage of the siScramble in each plate, was additionally used to analyse plate edge effects, as part of the data triage commonly used in image-based siRNA screens (Fig. 3B). Overall, we did not observe major changes in the cell number in relation to the well position in the plate (Fig. 3B), thereby excluding the possibility of false-positives/negatives due to

variations in cell growth. Similar results were observed for the plates of the combined siRNAs (data not shown). Next, we evaluated whether the data was reproducible across the four replicas. To this end, we calculated Pearson correlations to measure the linear correlation between the values of the percentage of infection for the four experiments, sequentially, in groups of two (Fig. 3C). In 5 out of 6 comparisons, a positive and significant correlation was observed, which is indicative of reproducibility among data sets (Fig. 3C). As a positive control, cells depleted for ATP6V1A were included in the screen. ATP6V1A is an important subunit of the vacuolar ATPase, which is responsible for endosomal acidification and therefore its silencing is expected to block DENV membrane fusion and hence infection (44). Surprisingly, however, ATP6V1A depletion did not significantly inhibit DENV infection or replication (Fig. 3D). This might suggest that sufficient knockdown with this particular siRNA was not achieved, or that redundant subunits or isoforms might participate in endosomal acidification, which is essential for DENV cell entry. Future experiments should be performed to reveal the knockdown efficiency of the siRNA pools towards ATPV1A in Huh7 cells by western blot analysis. Furthermore, flow cytometry experiments should validate the importance of ATPV1A in controlling DENV infection in comparison with lysosomotropic compounds such as ammonium chloride or bafilomycin A1, which are known to inhibit DENV infection (45,46). Lastly, we calculated the percentage of infected cells in the siScramble-transfected wells. The percentage of infection was 42.2% ± 2.4, which is higher than expected but still allowed us to monitor enhancement and inhibition of infection (Fig. 3E). Next, the number of infected cells (percentage of GFP-positive cells), the GFP intensity per well, and the GFP intensity of infected cells for all siRNA pools were determined. Statistical significance was assessed using the Z-score method. Z-scores represent the number of standard deviations that a value has from the mean or median, and they are frequently used to normalize data in a way that provides explicit information on the strength of each siRNA relative to the rest of the sample distribution (47). Figure 4A shows the Z-score distribution of the samples as compared to the siScramble based on the three assessed parameters. It becomes immediately evident that only a minor fraction of the ATG proteins and autophagy receptors significantly influenced DENV infection upon depletion.

Figure 3. Data triage of the siRNA screen results. (A) Distribution plot depicting the average number of cells per knockdown condition in the screen. Error bars represent SEM, the siScramble is indicated in red. **(B)** Heat-maps for each replica of the siRNA screen representing the number of cells per well, expressed as percentage of the siScramble-transfected cells, and shown in the scheme of the 96-well plates used for the screen. Only plates of the individual knockdowns are shown. **(C)** Pearson correlations between experiments based on the calculated percentages of infection (expressed as a fold change compared to the siScramble) of all the individual knockdowns. **(D)** Bar plot showing the percentage of infection (expressed as a fold change compared to the siScramble) of cells transfected with siATPV1A for the three measured parameters in the screen. **(E)** Bar plot showing the percentage of infected cells prior transfected with siScramble in the four screen repeats. Data represents mean ± SEM based on 4 technical replicates per experiment. Data in (A) and (D) represents mean ± SEM based on n=4.

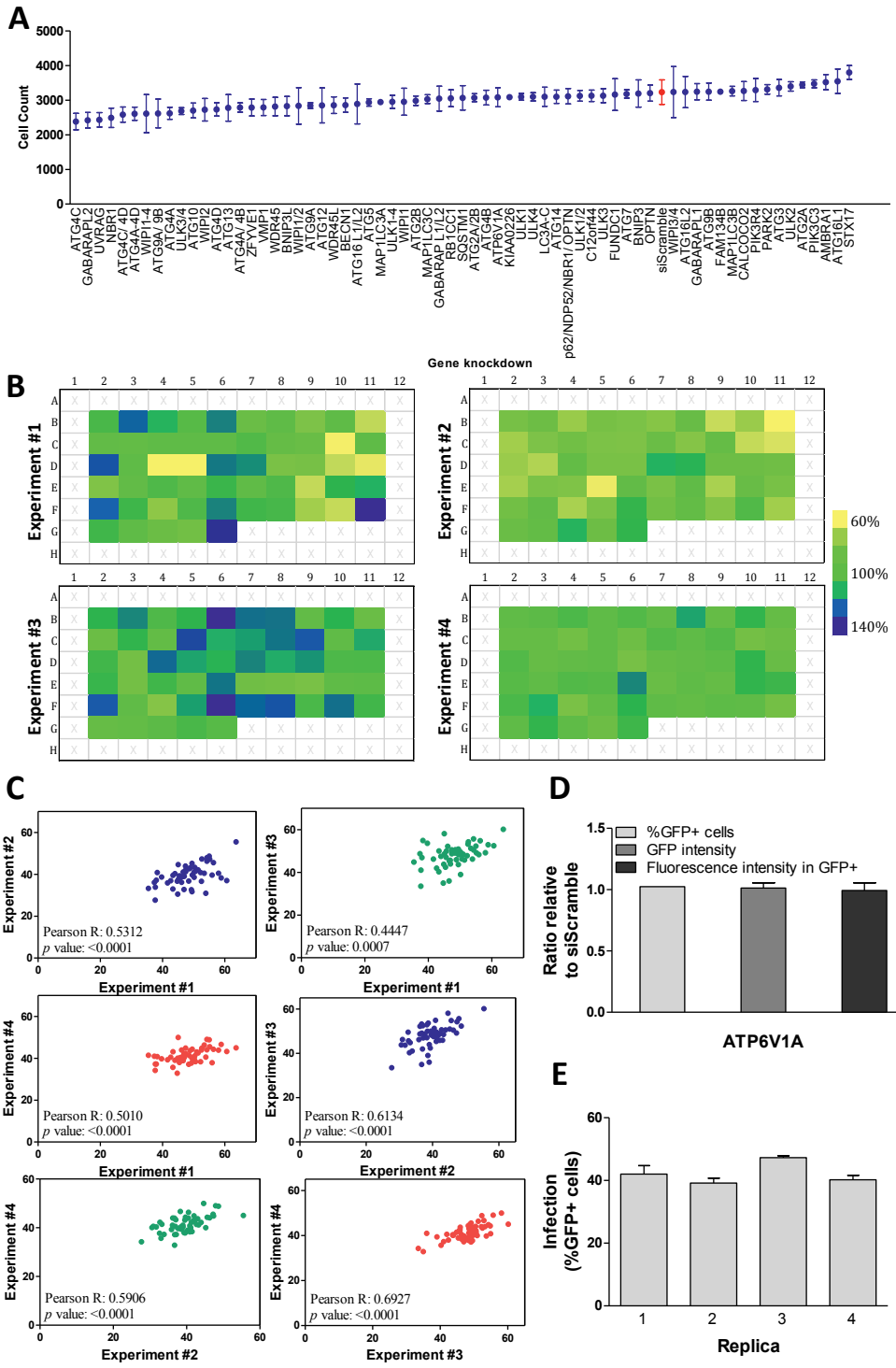
A
Cell Count
5000
4000
3000
2000
1000
0
ATG4C
GABARAPL2
UVRAG
NBR1
ATG4C/ 4D
ATG4A-4D
WIPI1-4
ATG9A/ 9B
ATG4A
ULK4
ATG10
WIPI2
ATG4D
ATG13
ATG4A/ 4B
ZFYVE1
VMP1
WDR45
BNIP1/2
WIPI1/2
ATG9A
ATG12
WDR45L
BECN1
ATG16 L1/L2
ATG5
MAP1LC3A
WIPI1/4
UVRAG
ATG2B
MAP1LC3C
GABARAPL1/L2
RB1CC1
SQSTM1
ATG2A/2B
ATG4B
ATP6V1A
KIAA0226
ULK1
ULK4
LC3A-C
ATG14
p62/NDP52/NBR1/OPTN
ULK1/2
C12orf44
ULK3
FUNDC1
ATG7
BNIP3
OPTN
siScramble
WIPI3/4
ATG16L2
GABARAPL1
ATG9B
FAM134B
MAP1LC3B
CALCOCO2
PIK3R4
PARK2
ATG3
ULK2
ATG2A
PIK3C3
AMBRA1
ATG16L1
STX17
B
Gene knockdown
Experiment #1
Experiment #2
Experiment #3
Experiment #4
60%
100%
140%
C
Experiment #2
Experiment #1
Pearson R: 0.5312
p value: <0.0001
Experiment #3
Experiment #1
Pearson R: 0.4447
p value: 0.0007
Experiment #4
Experiment #1
Pearson R: 0.5010
p value: <0.0001
Experiment #3
Experiment #2
Pearson R: 0.6134
p value: <0.0001
Experiment #4
Experiment #2
Pearson R: 0.5906
p value: <0.0001
Experiment #4
Experiment #3
Pearson R: 0.6927
p value: <0.0001
D
%GFP+ cells
GFP intensity
Fluorescence intensity in GFP+
Ratio relative to siScramble
1.5
1.0
0.5
0.0
ATP6V1A
E
Infection (%GFP+ cells)
60
40
20
0
1
2
3
4
Replica

Intriguingly, however, all of the identified 'hits' ($p<0.05$, Z-score $>+1.96$ for any of the three parameters; 11 out of 50 individual ATG protein/autophagy receptors knockdowns) appeared to have a restricting role in DENV infection, since all of them enhanced DENV replication and/or infection during knock-down conditions (Fig. 4B). Depletion of ATG4C was observed to significantly enhance DENV replication across all parameters tested (%GFP+ cells, the GFP intensity and the GFP intensity of the infected cells), indicating that this protein might interfere with viral infection and replication when it is normally expressed in the cell (Fig. 4A-B). Furthermore, in case of the redundant ATG protein depletions, simultaneous knockdown of all the isoforms of ATG4 favoured the number of DENV-infected cells and this difference was statistically significant as compared to the control cells (Fig. 4B). ATG4D and MAPLC3A knockdown led to a significant enhancement in the GFP intensity of the infected cells and the total GFP intensity, suggesting that these factors actively control viral replication. Depletion of ATG10, ATG13, ZFYVE1 and UVRAG specifically upregulated the GFP intensity of the GFP-positive cells, suggesting a role in viral replication. In the case of MAPLC3C and ATG2B silencing, a significant enhancement in the overall GFP intensity was observed. In both cases, also a trend to an enhancement in the other two parameters was seen. Similarly, BECN1 knockdown significantly increased the number of DENV-infected cells, with a tendency to upregulation of the overall GFP intensity. Interestingly, one protein, i.e., NBR1, decreased the number of infected cells ($p<0.05$, Z-score <-1.96; Fig. 4A-B) while at the same time increased GFP intensity in the GFP-positive cells ($p<0.05$, Z-score $>+1.96$; Fig. 4A-B).

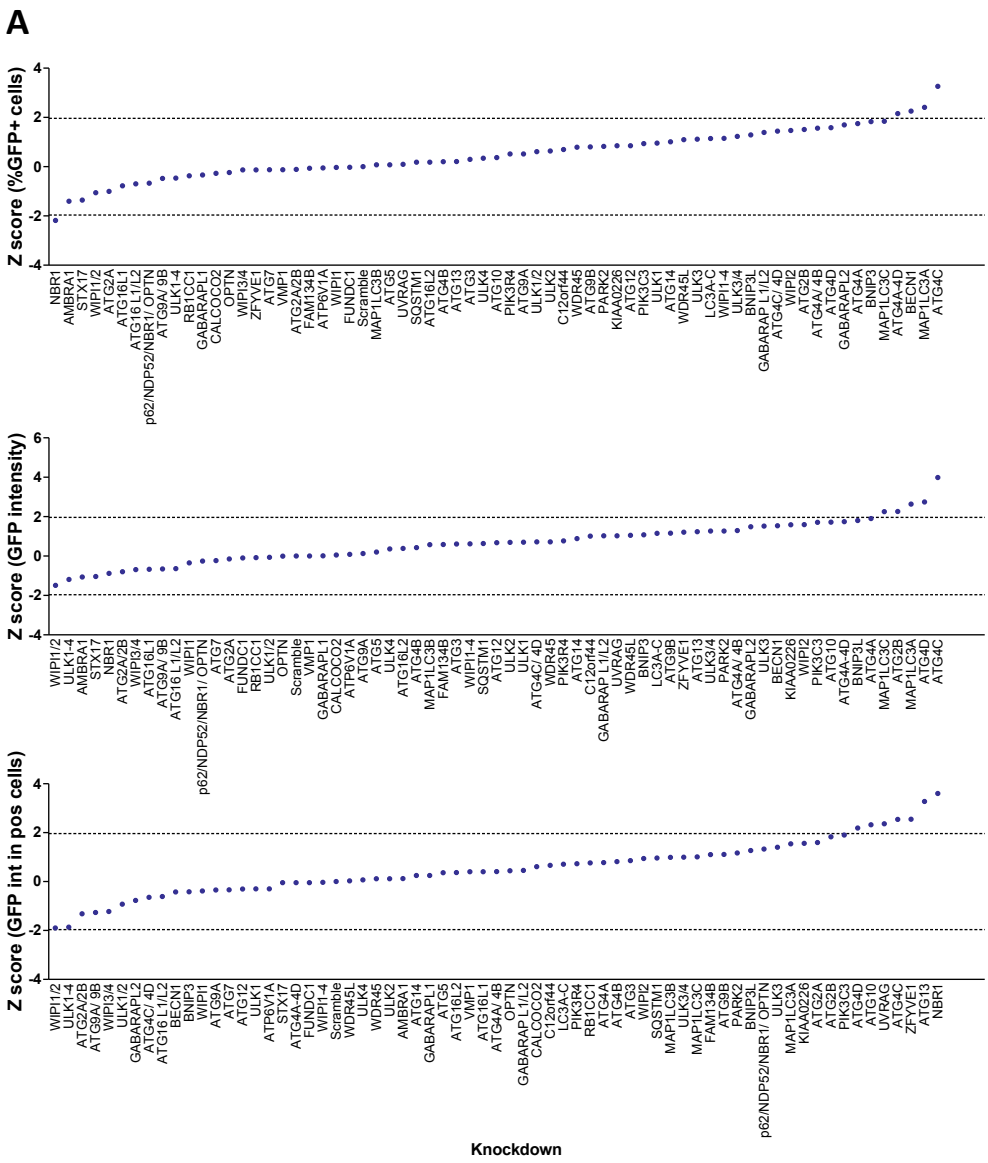

Figure 4. Analysis of the results of the siRNA-based screen for ATG proteins and specific autophagy receptors involved in DENV-infection. (A) Distribution plots of the Z-score values as compared to the siScramble control based on the percentage of GFP-positive cells (%), the GFP intensity per well and the GFP intensity in infected cells. Values for all the gene knockdowns included in the screen are shown. Z-scores between -1.96 and +1.96 represent significant hits with p <0.05. **(B)** Heat-map representing the ratio of GFP-positive cells (%), the average GFP intensity per well, and the average GFP intensity in infected cells, for each gene knockdown as compared to cells transfected with a siRNA scramble (bottom). The significant hits (p < 0.05 in at least one of the parameters) are indicated with a star.

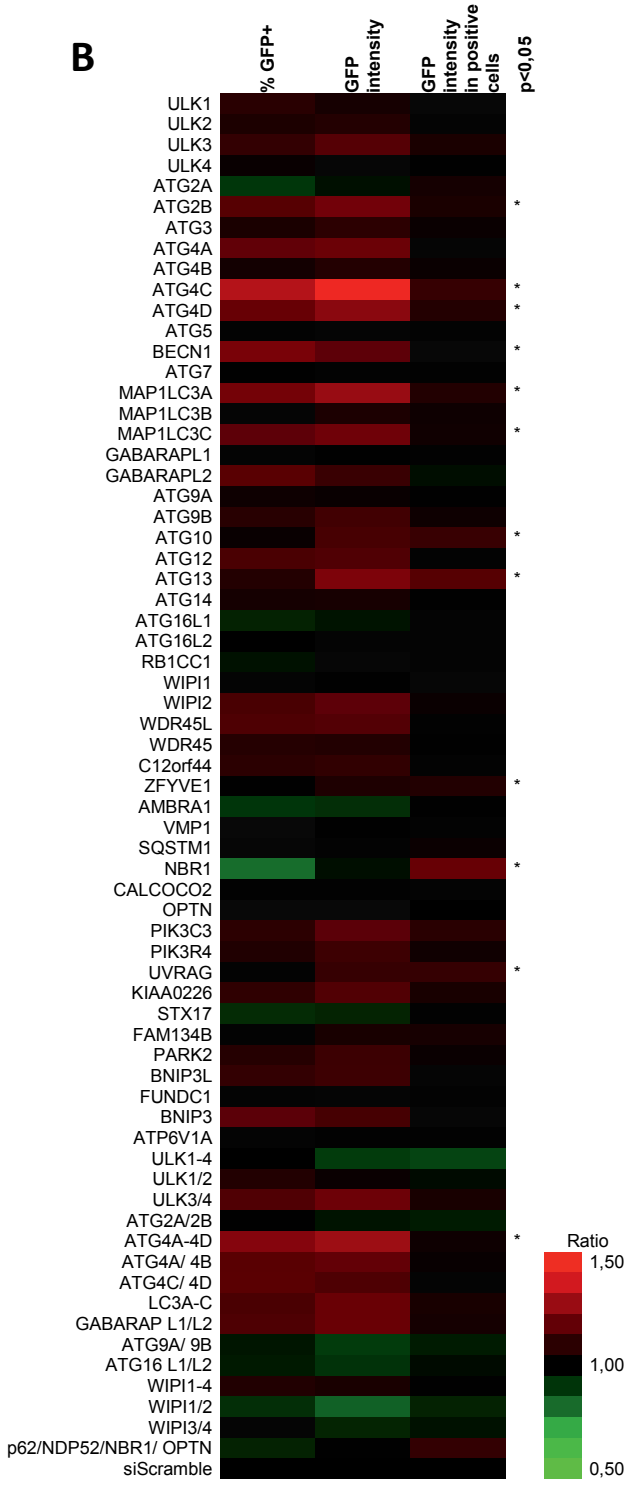
B
% GFP+
GFP intensity
GFP intensity in positive cells
p<0,05
ULK1
ULK2
ULK3
ULK4
ATG2A
ATG2B
ATG3
ATG4A
ATG4B
ATG4C
ATG4D
ATG5
BECN1
ATG7
MAP1LC3A
MAP1LC3B
MAP1LC3C
GABARAPL1
GABARAPL2
ATG9A
ATG9B
ATG10
ATG12
ATG13
ATG14
ATG16L1
ATG16L2
RB1CC1
WIPI1
WIPI2
WDR45L
WDR45
C12orf44
ZFYVE1
AMBRA1
VMP1
SQSTM1
NBR1
CALCOCO2
OPTN
PIK3C3
PIK3R4
UVRAG
KIAA0226
STX17
FAM134B
PARK2
BNIP3L
FUNDC1
BNIP3
ATP6V1A
ULK1-4
ULK1/2
ULK3/4
ATG2A/2B
ATG4A-4D
ATG4A/ 4B
ATG4C/ 4D
LC3A-C
GABARAP L1/L2
ATG9A/ 9B
ATG16 L1/L2
WIPI1-4
WIPI1/2
WIPI3/4
p62/NDP52/NBR1/ OPTN
siScramble
Ratio
1,50
1,00
0,50

From the hits in the primary screen, two ATG proteins were selected for further validation, i.e., ATG4C and NBR1, because these hits showed the most pronounced effect in the screen. Validation was performed by siRNA pool deconvolution (42). To this end, the individual siRNAs present in the siRNA pool were used for transfection and DENV infectivity was measured under the same experimental conditions as in the primary screen, but the readout was done by flow cytometry. In addition, cell viability was assessed by use of a viability dye. Fig. 5A shows a representative flow cytometry dot plot for cells transfected with the siScramble control at 28 hpi. Under the condition of the experiments, and in line with the screen results, 51.2% ± 9.3 of the siScramble transfected cells were infected with DENV. Silencing of ATG4C using the siRNA pool led to a 1.4-fold increase in the number of infected cells and these results are comparable to those obtained in the screen (Fig. 5B). However, in 3 out of 4 individual siRNAs no difference was seen when compared to the control. Only siRNA2 increased the percentage of infection to comparable levels as the siRNA pool (Fig. 5B). Analogously, silencing of NBR1with the pooled siRNAs decreased the percentage of DENV infection similar as in the primary siRNA screen (0.73-fold change as compared to the siScramble) yet again only one of the siRNAs present in the pool appeared to be responsible for this effect (Fig. 5C). Future studies should assess the knock-down efficiency of the single siRNAs to determine whether the enhanced DENV replication observed with one of the individual siRNAs targeting ATG4C and NBR1 are due to a better protein depletion or an off-target effect.

4. Discussion

Given the controversies surrounding the study of autophagy and more specifically the role of ATG proteins and receptors during DENV infection, we performed a siRNA screen to determine the role of the ATG proteome and selected autophagy receptors in DENV infection and replication. Overall, we observed a limited effect of the ATG proteome depletion on DENV infection. The two most prominent hits were ATG4C and NBR1. ATG4C silencing was found to increase DENV infection and replication whereas NBR1 silencing reduced the number of infected cells, yet the cells that were infected had enhanced GFP expression levels compared to the control. The validation experiments performed so far, however, could not confirm that both ATG4C and NBR1 are true hits as in the deconvolution experiments only 1 out of 4 individual siRNAs reproduced the effect observed for the siRNA pool. Future experiments are required to validate these hits in more detail.

When only 1 of 4 different siRNAs present in the pool is responsible for the effect observed in the siRNA screen, the protein involved is often considered as a false positive hit. siRNAs are known to have off target effects, i.e., they deplete different genes that the one intended, and the higher the concentration used for the knockdown, the higher the chance to have these effects (48). However, the concentration of the siRNAs used here is considered low, i.e., 20 nM and 5 nM for the siRNA pool and each single siRNA, respectively. To prove or disprove NBR1 and ATG4C as factors that control DENV infection, it is important to determine the knockdown efficiency of the siRNA that is having an effect on viral replication in comparison to the other siRNAs present in the pool, and to examine whether the reduction of the protein levels correlates with the

results observed in terms of the infection. A different strategy used successfully by others for validation of hits of a primary siRNA screen is to use reagents from a different company for a secondary screen (49). Generation of a knockout cell line using the CRISP/Cas9 technology also offers an alternative strategy.

The siRNA pool targeting NBR1 results in an intriguing phenotype as it was observed to promote virus infection (siRNA transfection decreased the number of GFP-positive cells), yet once infection is established limits viral replication (siRNA transfection increased GFP intensity in infected cells). This may imply that distinct signalling pathways are under the control of this protein, which would be activated at different times in infection. Similarly, to p62, NBR1 is an autophagy receptor that facilitates the selective degradation of ubiquitinated misfolded proteins (50) and peroxisomes (51) by autophagy. Given the antiviral function that has been described for p62 (32), it might be possible that NBR1 controls DENV replication in a similar fashion. Indeed, NBR1 has been reported to contribute to selective autophagic degradation of viruses in plants, by targeting non-assembled and virus particle-forming capsid proteins to autophagosomes (52). In case that the siRNA pool does not target NBR1, multiple approaches can be taken to unveil the protein or proteins depleted by this probe and involved in controlling DENV infection. For example, *in silico* modelling can be used for identification of potential targets, followed by experimental validation of the identified transcripts. Alternatively, global quantitative proteomic analysis or RNA sequencing of cells transfected solely with the concerned siRNA in comparison to cells transfected with any of the other siRNAs present in the pool can be performed.

In the case of ATG4C, we observed that silencing of this protein had a positive effect in DENV infection and replication. Interestingly, simultaneous depletion of the four isoforms of this protein was also shown to significantly favour viral replication in the screen. ATG4 proteins are part of the same protease family that is involved in the cleavage of the C-terminus of cytoplasmic LC3 to expose a glycine residue, prior its conjugation to PE (53). ATG4 isoforms have a dual role, as they are also responsible for the de-conjugation of LC3-II from the autophagic membrane (53). Whereas ATG4A and ATG4B perform the aforementioned functions, ATG4C and ATG4D have been shown to be less active. Furthermore, recent data suggests that ATG4D is negatively regulated by reactive oxygen species and that this protein is subjected to caspase-mediated cleavage to increases its activity (54,55). It would be therefore interesting to investigate how the different isoforms of ATG4 contribute to DENV infection, especially since oxidative damage and caspase-mediated cell death are both mechanisms associated with the cellular response to this virus.

The observation that only a limited set of proteins control DENV infection suggests that autophagy is not required for infection and that the identified proteins regulate DENV infection via unconventional roles outside autophagy. We found that depletion of ATG2B, ATG4D, LC3C, ATG10, ATG13, ZFYVE1, and UVRAG increased the GFP intensity, which suggests that these proteins might interfere with viral replication. To the best of our knowledge, none of the aforementioned proteins have been reported before in the context of DENV infection, reason why further research is encouraged. Furthermore, recent research demonstrates that some of these proteins indeed modulate the infectivity of other viruses. For example, ATG2B silencing causes clustering of enlarged lipid droplets in an autophagy-independent manner (56), and was found upregulated

during Japanese Encephalitis virus infection, another flavivirus (57). Interestingly, regulation of the lipid content of the cell through mechanisms dependent and independent of autophagy during DENV infection have been reported (35,58,59). On the other hand, UVRAG, a membrane trafficking protein, is involved in Influenza A virus and Vesicular Stomatitis virus entry (60), and ZFYVE1 might potentially be involved in viral infections in a similar fashion (61).

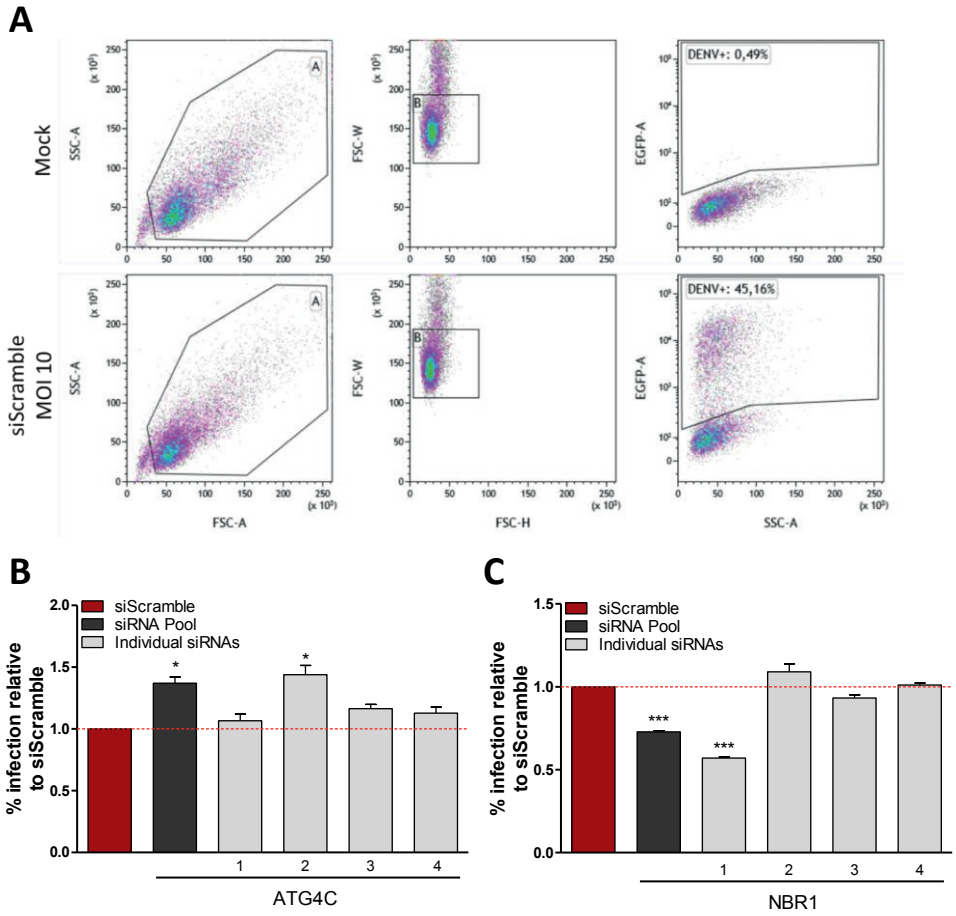

Figure 5. Validation of ATG4C and NBR1 as potential factors involved in DENV infection by standard siRNA pool deconvolution. Huh7 cells were reverse-transfected with pooled or individual siRNAs targeting the indicated genes for 48 h prior to infection as described in the legend to Figure 2 but the format was scaled to 24 well plates. Cells were harvested and analyzed for GFP expression by flow cytometry. **(A)** Representative dot plots showing the gating strategy of infected cells (i.e., GFP-positive cells). **(B and C)** Bar plots showing the percentage of infection relative to that of siScramble-transfected cells. (B) ATG4C and (C) NBR1 knockdown. Data represents mean ± SEM of n = 3. Student's test: *** $p < 0.001$, * $p < 0.05$.

Multiple ATG proteins appear to restrict DENV infection yet the effect measured was rather limited under the conditions of the screen. In future studies, we therefore propose to decrease the MOI used such that a maximal effect can be measured. Also, at lower MOI conditions, infection can be continued for multiple rounds of infection to

potentially amplify the observed effect. Furthermore, read-outs to assess the viral replication cycle such as the quantification of the number of infectious particles or genome equivalent copies could also be integrated in the screening procedure, as this will unveil the potential roles of ATG proteins in processes downstream of viral genome replication, transcription and translation.

In conclusion, we aimed to better understand the relationship between the core ATG proteome and selected autophagy receptors, and DENV infection. The study of autophagy and its components during DENV infection has proven to be challenging as many contrasting observations have been reported (this thesis, **Chapter 2**). The investigation of the hits obtained in our screen could help to shed some light on these controversies.

References

1. Dick OB, San Martín JL, Montoya RH, Del Diego J, Zambrano B, Dayan GH. Review: The history of dengue outbreaks in the Americas. Am J Trop Med Hyg. 2012 Oct;87(4):584–93.
2. Bhatt S, Gething PW, Brady OJ, Messina JP, Farlow AW, Moyes CL, et al. The global distribution and burden of dengue. Nature. 2013 Apr 25;496(7446):504–7.
3. Wilder-Smith A, Gubler DJ, Weaver SC, Monath TP, Heymann DL, Scott TW. Epidemic arboviral diseases: priorities for research and public health. Lancet Infect Dis. 2017 Mar 1;17(3):e101–6.
4. Herrero LJ, Zakhary A, Gahan ME, Nelson MA, Herring BL, Hapel AJ, et al. Dengue virus therapeutic intervention strategies based on viral, vector and host factors involved in disease pathogenesis. Pharmacol Ther. 2013 Feb;137(2):266–82.
5. Huy NT, Van Giang T, Thuy DHD, Kikuchi M, Hien TT, Zamora J, et al. Factors Associated with Dengue Shock Syndrome: A Systematic Review and Meta-Analysis. PLoS Negl Trop Dis. 2013 Jan 26;7(9):e2412.
6. Whitehead SS, Subbarao K. Which Dengue Vaccine Approach Is the Most Promising, and Should We Be Concerned about Enhanced Disease after Vaccination? Cold Spring Harb Perspect Biol. 2018 Jun 1;10(6):a028811.
7. Dans AL, Dans LF, Lansang MAD, Silvestre MAA, Guyatt GH. Controversy and debate on dengue vaccine series—paper 1: review of a licensed dengue vaccine: inappropriate subgroup analyses and selective reporting may cause harm in mass vaccination programs. Vol. 95, Journal of Clinical Epidemiology. 2018. p. 137–9.
8. Johnson AJ, Guirakhoo F, Roehrig JT. The envelope glycoproteins of dengue 1 and dengue 2 viruses grown in mosquito cells differ in their utilization of potential glycosylation sites. Virology. 1994 Sep;203(2):241–9.
9. Pokidysheva E, Zhang Y, Battisti AJ, Bator-Kelly CM, Chipman PR, Xiao C, et al. Cryo-EM reconstruction of dengue virus in complex with the carbohydrate recognition domain of DC-SIGN. Cell. 2006 Feb 10;124(3):485–93.
10. Villordo SM, Gamarnik A V. Genome cyclization as strategy for flavivirus RNA replication. Virus Res. 2009 Feb;139(2):230–9.
11. Lescar J, Luo D, Xu T, Sampath A, Lim SP, Canard B, et al. Towards the design of antiviral inhibitors against flaviviruses: The case for the multifunctional NS3 protein from Dengue virus as a target. Antiviral Res. 2008 Nov;80(2):94–101.
12. Acosta EG, Castilla V, Damonte EB. Alternative infectious entry pathways for dengue virus serotypes into mammalian cells. Cell Microbiol. 2009 Oct;11(10):1533–49.
13. Acosta EG, Castilla V, Damonte EB. Differential Requirements in Endocytic Trafficking for Penetration of Dengue Virus. PLoS One. 2012 Jan 7;7(9):e44835.
14. Perera R, Khaliq M, Kuhn RJ. Closing the door on flaviviruses: Entry as a target for antiviral drug design. Vol. 80, Antiviral Research. 2008. p. 11–22.
15. Paul D, Bartenschlager R. Flaviviridae Replication Organelles: Oh, What a Tangled Web We Weave. Annu Rev Virol. 2015 Nov 6;2(1):289–310.
16. Gopala Reddy SB, Chin W-X, Shivananju NS. Dengue virus NS2 and NS4: Minor proteins, mammoth roles. Biochem Pharmacol. 2018 Aug 1;154:54–63.
17. Chen S, Wu Z, Wang M, Cheng A. Innate immune evasion mediated by flaviviridae non-structural proteins. Viruses. 2017;9(10).
18. Perera R, Kuhn RJ. Structural proteomics of dengue virus. Curr Opin Microbiol. 2008 Aug;11(4):369–77.
19. Urcuqui-Inchima S, Patiño C, Torres S, Haenni A-L, Díaz FJ. Recent Developments in Understanding Dengue Virus Replication. In: Advances in virus research. 2010. p. 1–39.
20. Rodenhuis-Zybert IA, Wilschut J, Smit JM. Dengue virus life cycle: viral and host factors modulating infectivity. Cell Mol Life Sci. 2010 Aug;67(16):2773–86.
21. Rey-Jurado E, Riedel CA, González PA, Bueno SM, Kalergis AM. Contribution of autophagy to antiviral immunity. FEBS Lett. 2015 Nov 14;589(22):3461–70.
22. Bento CF, Renna M, Ghislat G, Puri C, Ashkenazi A, Vicinanza M, et al. Mammalian autophagy: how does it work? Annu Rev Biochem. 2016;85(1):685–713.
23. Mizushima N, Yoshimori T, Ohsumi Y. The Role of Atg Proteins in Autophagosome Formation. Annu Rev Cell Dev Biol. 2011 Nov 10;27(1):107–32.
24. Wong PM, Feng Y, Wang J, Shi R, Jiang X. Regulation of autophagy by coordinated

action of mTORC1 and protein phosphatase 2A. Nat Commun. 2015 Dec 27;6(1):8048.
25. Chiramel A, Brady N, Bartenschlager R. Divergent Roles of Autophagy in Virus Infection. Cells. 2013 Jan 25;2(1):83–104.
26. Nakatogawa H. Two ubiquitin-like conjugation systems that mediate membrane formation during autophagy. Essays Biochem. 2013 Sep 27;55:39–50.
27. Ichimura Y, Kirisako T, Takao T, Satomi Y, Shimonishi Y, Ishihara N, et al. A ubiquitin-like system mediates protein lipidation. Nature. 2000 Nov 23;408(6811):488–92.
28. Behrends C, Fulda S. Receptor proteins in selective autophagy. Int J Cell Biol. 2012;2012:673290.
29. Kabeya Y. LC3, a mammalian homologue of yeast Apg8p, is localized in autophagosome membranes after processing. EMBO J. 2000 Nov 1;19(21):5720–8.
30. Yoshii SR, Mizushima N. Monitoring and measuring autophagy. Int J Mol Sci. 2017 Aug 28;18(9).
31. McLean JE, Wudzinska A, Datan E, Quaglino D, Zakeri Z. Flavivirus NS4A-induced autophagy protects cells against death and enhances virus replication. J Biol Chem. 2011 Jun 24;286(25):22147–59.
32. Metz P, Chiramel A, Chatel-Chaix L, Alvisi G, Bankhead P, Mora-Rodríguez R, et al. Dengue Virus inhibition of autophagic flux and dependency of viral replication on proteasomal degradation of the autophagy receptor p62. Diamond MS, editor. J Virol. 2015;89(15):8026–41.
33. Majzoub K, Bird SW, van Buuren N, Kirkegaard K, Abernathy E, Mateo R, et al. Differential and convergent utilization of autophagy components by positive-strand RNA viruses. Sugden B, editor. PLOS Biol. 2019 Jan 4;17(1):e2006926.
34. Lee YR, Lei HY, Liu MT, Wang JR, Chen SH, Jiang-Shieh YF, et al. Autophagic machinery activated by dengue virus enhances virus replication. Virology. 2008 May 10;374(2):240–8.
35. Heaton NS, Randall G. Dengue virus-induced autophagy regulates lipid metabolism. Cell Host Microbe. 2010 Nov 18;8(5):422–32.
36. Mauthe M, Langereis M, Jung J, Zhou X, Jones A, Omta W, et al. An siRNA screen for ATG protein depletion reveals the extent of the unconventional functions of the autophagy proteome in virus replication. J Cell Biol. 2016 Aug 29;214(5):619–35.
37. Mauthe M, Reggiori F. ATG proteins: Are we always looking at autophagy? Autophagy. 2016 Dec 23;12(12):2502–3.
38. Subramani S, Malhotra V. Non-autophagic roles of autophagy-related proteins. EMBO Rep. 2013 Feb;14(2):143–51.
39. Fischl W, Bartenschlager R. High-Throughput Screening Using Dengue Virus Reporter Genomes. In: Methods in molecular biology (Clifton, NJ). 2013. p. 205–19.
40. Ayala-Nuñez N V., Wilschut J, Smit JM. Monitoring virus entry into living cells using DiD-labeled dengue virus particles. Methods. 2011 Oct 1;55(2):137–43.
41. Suksanpaisan L, Cabrera-Hernandez A, Smith DR. Infection of human primary hepatocytes with dengue virus serotype 2. J Med Virol. 2007 Mar;79(3):300–7.
42. Sigoillot FD, King RW. Vigilance and validation: Keys to success in RNAi screening. ACS Chem Biol. 2011 Jan 21;6(1):47–60.
43. Diosa-Toro M, Troost B, van de Pol D, Heberle AM, Urcuqui-Inchima S, Thedieck K, et al. Tomatidine, a novel antiviral compound towards dengue virus. Antiviral Res. 2019 Jan;161:90–9.
44. Ho M-R, Tsai T-T, Chen C-L, Jhan M-K, Tsai C-C, Lee Y-C, et al. Blockade of dengue virus infection and viral cytotoxicity in neuronal cells in vitro and in vivo by targeting endocytic pathways. Sci Rep. 2017 Dec 31;7(1):6910.
45. Piccini LE, Castilla V, Damonte EB. Dengue-3 Virus Entry into Vero Cells: Role of Clathrin-Mediated Endocytosis in the Outcome of Infection. Jin X, editor. PLoS One. 2015 Oct 15;10(10):e0140824.
46. Wu YW, Mettling C, Wu SR, Yu CY, Perng GC, Lin YS, et al. Autophagy-associated dengue vesicles promote viral transmission avoiding antibody neutralization. Sci Rep. 2016 Oct 25;6(1):32243.
47. Birmingham A, Selfors LM, Forster T, Wrobel D, Kennedy CJ, Shanks E, et al. Statistical methods for analysis of high-throughput RNA interference screens. Nat Methods. 2009 Aug;6(8):569–75.
48. Caffrey DR, Zhao J, Song Z, Schaffer ME, Haney SA, Subramanian RR, et al. siRNA Off-Target Effects Can Be Reduced at Concentrations That Match Their Individual Potency. Preiss T, editor. PLoS One. 2011 Jul 5;6(7):e21503.
49. Li MMH, Lau Z, Cheung P, Aguilar EG, Schneider WM, Bozzacco L, et al. TRIM25 Enhances the Antiviral Action of Zinc-Finger Antiviral Protein (ZAP). Fernandez-Sesma A, editor. PLOS Pathog. 2017 Jan 6;13(1):e1006145.

50. Kirkin V, Lamark T, Sou Y-S, Bjørkøy G, Nunn JL, Bruun J-A, et al. A Role for NBR1 in Autophagosomal Degradation of Ubiquitinated Substrates. Mol Cell. 2009 Feb;33(4):505–16.
51. Deosaran E, Larsen KB, Hua R, Sargent G, Wang Y, Kim S, et al. NBR1 acts as an autophagy receptor for peroxisomes. J Cell Sci. 2013 Feb 15;126(4):939–52.
52. Hafrén A, Hofius D. NBR1-mediated antiviral xenophagy in plant immunity. Autophagy. 2017 Nov 2;13(11):2000–1.
53. Kauffman KJ, Yu S, Jin J, Mugo B, Nguyen N, O'Brien A, et al. Delipidation of mammalian Atg8-family proteins by each of the four ATG4 proteases. Autophagy. 2018 Apr 10;1–19.
54. Scherz-Shouval R, Shvets E, Fass E, Shorer H, Gil L, Elazar Z. Reactive oxygen species are essential for autophagy and specifically regulate the activity of Atg4. EMBO J. 2007 Apr 4;26(7):1749–60.
55. Betin VMS, Lane JD. Caspase cleavage of Atg4D stimulates GABARAP-L1 processing and triggers mitochondrial targeting and apoptosis. J Cell Sci. 2009 Jul 15;122(14):2554–66.
56. Velikkakath AKG, Nishimura T, Oita E, Ishihara N, Mizushima N. Mammalian Atg2 proteins are essential for autophagosome formation and important for regulation of size and distribution of lipid droplets. Mol Biol Cell. 2012 Mar;23(5):896–909.
57. Sharma M, Bhattacharyya S, Nain M, Kaur M, Sood V, Gupta V, et al. Japanese encephalitis virus replication is negatively regulated by autophagy and occurs on LC3-I- and EDEM1-containing membranes. Autophagy. 2014 Sep 19;10(9):1637–51.
58. Zhang J, Lan Y, Li MY, Lamers MM, Fusade-Boyer M, Klemm E, et al. Flaviviruses Exploit the Lipid Droplet Protein AUP1 to Trigger Lipophagy and Drive Virus Production. Cell Host Microbe. 2018 Jun 13;23(6):819-831.e5.
59. Randall G. Lipid Droplet Metabolism during Dengue Virus Infection. Trends Microbiol. 2018 Aug 1;26(8):640–2.
60. Pirooz SD, He S, Zhang T, Zhang X, Zhao Z, Oh S, et al. UVRAG is required for virus entry through combinatorial interaction with the class C-Vps complex and SNAREs. Proc Natl Acad Sci. 2014 Feb 18;111(7):2716–21.
61. Bernard A, Klionsky DJ. Defining the membrane precursor supporting the nucleation of the phagophore. Autophagy. 2014 Jan 20;10(1):1–2.

Supplementary data

Table S1. Genes targeted by the customized siRNA library

Gene Symbol	Gene ID	Gene Accession
ULK1	8408	NM_003565
ULK2	9706	NM_014683
ULK3	25989	NM_015518
ULK4	54986	XM_929989
ATG2A	23130	NM_015104
ATG2B	55102	NM_018036
ATG3	64422	NM_022488
ATG4A	115201	NM_178270
ATG4B	23192	NM_013325
ATG4C	84938	NM_178221
ATG4D	84971	NM_032885
ATG5	9474	NM_004849
BECN1	8678	NM_003766
ATG7	10533	NM_006395
MAP1LC3A	84557	NM_181509
MAP1LC3B	81631	NM_022818
MAP1LC3C	440738	NM_001004343
GABARAPL1	23710	NM_031412
GABARAPL2	11345	NM_007285
ATG9A	79065	NM_024085
ATG9B	285973	NM_173681
ATG10	83734	NM_031482
ATG12	9140	NM_004707
ATG13	9776	NM_014741
ATG14	22863	NM_014924
ATG16L1	55054	NM_198890
ATG16L2	89849	NM_033388
RB1CC1	9821	NM_014781
WIPI1	55062	NM_017983
WIPI2	26100	NM_001033520
WDR45B	56270	NM_019613
WDR45	11152	NM_001029896
ATG101	60673	NM_021934
ZFYVE1	53349	NM_178441
AMBRA1	55626	NM_017749
VMP1	81671	NM_030938
SQSTM1	8878	NM_003900
NBR1	4077	NM_005899
CALCOCO2	10241	NM_005831
OPTN	10133	NM_021980
PIK3C3	5289	NM_002647
PIK3R4	30849	NM_014602
UVRAG	7405	NM_003369
KIAA0226	9711	XM_032901
STX17	55014	NM_017919
FAM134B	54463	NM_019000
PARK2	5071	NM_013988
BNIP3L	665	NM_004331
FUNDC1	139341	NM_173794
BNIP3	664	NM_004052
ATP6V1A	523	NM_001690